Journal of Pharmaceutical Analysis 10 (2020) 546–559

Contents lists available at ScienceDirect

Journal of Pharmaceutical Analysis

journal homepage: www.elsevier.com/locate/jpa

Original article

Discovery of human coronaviruses pan-papain-like protease inhibitors using computational approaches

Mubarak A. Alamri [a, *, 1], Muhammad Tahir ul Qamar [b, 1], Muhammad Usman Mirza [c, 1], Safar M. Alqahtani [a], Matheus Froeyen [c], Ling-Ling Chen [b, d, **]

[a] Department of Pharmaceutical Chemistry, College of Pharmacy, Prince Sattam Bin Abdulaziz University, Alkarj, Saudi Arabia
[b] College of Life Science and Technology, Guangxi University, Nanning, China
[c] Department of Pharmaceutical and Pharmacological Sciences, Rega Institute for Medical Research, Medicinal Chemistry, University of Leuven, B-3000, Leuven, Belgium
[d] Hubei Key Laboratory of Agricultural Bioinformatics, College of Informatics, Huazhong Agricultural University, Wuhan, 430070, China

ARTICLE INFO

Article history:
Received 25 March 2020
Received in revised form
23 August 2020
Accepted 24 August 2020
Available online 28 August 2020

Keywords:
COVID-19
MERS-CoV
Molecular dynamic simulation
Pan-inhibitors
Papain-like protease
SARS-CoV
SARS-CoV-2
Virtual screening

ABSTRACT

The papain-like protease (PL^{pro}) is vital for the replication of coronaviruses (CoVs), as well as for escaping innate-immune responses of the host. Hence, it has emerged as an attractive antiviral drug-target. In this study, computational approaches were employed, mainly the structure-based virtual screening coupled with all-atom molecular dynamics (MD) simulations to computationally identify specific inhibitors of severe acute respiratory syndrome coronavirus 2 (SARS-CoV-2) PL^{pro}, which can be further developed as potential pan-PL^{pro} based broad-spectrum antiviral drugs. The sequence, structure, and functional conserveness of most deadly human CoVs PL^{pro} were explored, and it was revealed that functionally important catalytic triad residues are well conserved among SARS-CoV, SARS-CoV-2, and middle east respiratory syndrome coronavirus (MERS-CoV). The subsequent screening of a focused protease inhibitors database composed of ~7,000 compounds resulted in the identification of three candidate compounds, ADM_13083841, LMG_15521745, and SYN_15517940. These three compounds established conserved interactions which were further explored through MD simulations, free energy calculations, and residual energy contribution estimated by MM-PB(GB)SA method. All these compounds showed stable conformation and interacted well with the active residues of SARS-CoV-2 PL^{pro}, and showed consistent interaction profile with SARS-CoV PL^{pro} and MERS-CoV PL^{pro} as well. Conclusively, the reported SARS-CoV-2 PL^{pro} specific compounds could serve as seeds for developing potent pan-PL^{pro} based broad-spectrum antiviral drugs against deadly human coronaviruses. Moreover, the presented information related to binding site residual energy contribution could lead to further optimization of these compounds.

1. Introduction

Coronaviruses (CoVs) are enveloped RNA viruses covered with a non-segmented positive-sense RNA genome of 28–30 kb, known since the mid-1960s [1]. These viruses can infect a variety of hosts and can cause different respiratory, enteric, liver, and systemic diseases [1,2]. CoVs have the potential to transmit among animals and humans [3,4], which is evident from previous CoVs outbreaks. The severe acute respiratory syndrome (SARS) surfaced in 2002/2003 and resulted in 800 deaths [5]. Soon after the rise of this new viral infection, several new CoVs were uncovered [6]. In 2012, Middle East respiratory syndrome coronavirus (MERS-CoV) was identified with the potential of human-to-human transmission [7,8]. The mortality rate of SARS-CoV and MERS-CoV was estimated to be around 15% for SARS-CoV [9] and 35% for MERS-CoV [10]. The currently emerged SARS-CoV-2 spread globally and turned into the pandemic of life threatening coronavirus disease-2019 (COVID-19) [11]. To date, various potential SARS-CoV-2 drug-targets have been reported, and various efforts have been made to identify potential

Peer review under responsibility of Xi'an Jiaotong University.
* Corresponding author.
** Corresponding author. College of Life Science and Technology, Guangxi University, Nanning, PR China.
E-mail addresses: m.alamri@psau.edu.sa (M.A. Alamri), llchen@mail.hzau.edu.cn (L.-L. Chen).
[1] These authors contributed equally in this study.

https://doi.org/10.1016/j.jpha.2020.08.012

therapeutics as presented in recent reviews [11–15].

SARS-CoV-2 belongs to beta-CoVs, and is based on 800-kDa polypeptide, which is cleaved into structural and non-structural proteins upon translation [16,17]. 3-chymotrypsin-like protease ($3CL^{pro}$) and papain-like protease (PL^{pro}) are active partners in mediating this proteolytic processing. CoVs PL^{pro} is grouped in the peptidase clan CA (family C16). The active site of PL^{pro} consists of a typical catalytic triad, comprising Cys111–His272–Asp286 residues. CoVs PL^{pro} is extensively studied, well-aligned, functional, and situated at the border of the thumb and palm sub-domains [18]. PL^{pro} performs its proteolytic functions through its catalytic cysteine-protease cycle, in which Cys111 functions as a nucleophile, His272 acts as a general acid/base and Asp286 is linked with the histidine assisting it to align and help deprotonation of Cys111 [19]. CoVs $3CL^{pro}$ and PL^{pro} mainly process the viral polyprotein. However, PL^{pro} has an extra role of extracting ISG15 and ubiquitin from the proteins of host-cell to help CoVs in the dodging of host-innate immune responses [19,20]. The C-terminal of ubiquitin molecule is suggested to accommodate a cleft in close proximity to the functional catalytic triad which consists of the conserved ubiquitin-specific protease residue, Asp 164, and two hydrophobic subsites S3 and S4. Targeting this pocket is preferable for the development of non-covalent SARS-CoV agents as it could allosterically block the active site by inducing loop closure [21]. Therefore, PL^{pro} is a significant target for anti-CoVs drug designing [22]. PL^{pro} based antiviral drugs may not only inhibit the CoVs replication cycle; they may also have an advantage in impeding the dysregulation of signalling cascades in CoVs infected cells, further leading to the death of un-infected neighbouring cells [19].

Up to date, there is no clinically approved drug or vaccine available to protect against recent COVID-19 [23,24]. For treating COVID-19 pneumonia, health officials are currently testing and evaluating existing anti-pneumonia treatments. Existing antivirals, including protease inhibitors (indinavir, saquinavir, and lopinavir/ritonavir), as well as RNA polymerase inhibitors, including remdesivir [25–27], are being tested against SARS-CoV-2. Recently, the in vitro antiviral competence analyses of a few FDA-approved as well as experimental drugs against clinical isolates of SARS-CoV-2, such as chloroquine and remdesivir, showed promising results [26]. However, to tackle the current COVID-19 pandemic, the development of wide-spectrum inhibitors against CoVs is a crucial strategy.

In recent years, the use of computational approaches for the discovery of small molecules has achieved importance in drug development [28–33]. Among various approaches, molecular docking has been extensively used for investigating the binding interactions of small molecules with the active sites of the target protein [34–38]. In antiviral drug discovery, hierarchical virtual screening approaches have already identified promising antiviral compounds against a broad range of viruses including influenza [39], Ebola [40–42], Dengue [43–48], Zika Virus [48–50] and recently against CoVs [22,51–53], while others display the significance of molecular dynamics (MD) simulations in search for possible antiviral [44,54–61] and investigated drug resistance mechanisms [54,58,62–64]. PL^{pro} is a highly conserved protease across CoVs [65] and considered as a potential target for SARS-CoV inhibitors with broad-spectrum antiviral activity [19]. In this contribution, a combined virtual screening approach and all-atom MD simulations were employed to investigate potential pan-PL^{pro} inhibitors that could be further developed into broad-spectrum anti-COVID-19 drugs.

2. Materials and methods

2.1. Proteins sequence and structure alignment

The functional evolutionary conserved residues of SARS-CoV, SARS-CoV-2 and MERS-CoV were recognized through sequence and structure alignments that could provide a structural motif for inhibitor design towards the discovery of pan-PL^{pro} based broad spectrum anti-COVID-19 hits. Sequence and 3D structures of SARS-CoV-2 PL^{pro} (Protein Data Bank (PDB): 6W9C), SARS-CoV PL^{pro} (PDB: 3MJ5), and MERS-CoV PL^{pro} (PDB: 4R3D) were retrieved from PDB [66]. Clustal Omega was used to align the PL^{pro} sequences [67]. Structure alignment analysis was performed using PyMOL 1.3. tool [68].

2.2. Chemical libraries preparation

The Asinex protease inhibitor library composed of 6,968 compounds in three-dimensional (3D) representation and structural data format (SDF) was downloaded from the Asinex platform (https://www.asinex.com/protease/). The compounds were imported, and energy minimized using MMFF94 force field implemented in Open Babel [69]. Then compounds were prepared for screening using Autodock Tools [70] by adding the polar hydrogens and computing the gasteiger charges. All the optimized compounds were then saved as PDBQT files format for further molecular docking studies.

2.3. Structure-based virtual screening and molecular docking

The x-ray structure of SARS-CoV-2 PL^{pro} in a resolution of 2.7 Å (PDB: 6W9C) was used for the docking purpose. Initially, the co-crystalized inhibitors and unwanted water molecules were removed by the Discovery Studio Visualizer [71]. The protein structure was prepared from PDB files into PDBQT using Autodock Tools. The polar-hydrogen atoms were included, and gasteiger charges were processed before docking. The structure-based virtual screening was carried out using Autodock-vina in PyRx 0.8 virtual screening tool [72]. Due to the high degree of sequence identity, the structure of SARS-CoV PL^{pro} (PDB: 3MJ5) bound to GRL-0667S, a non-covalent inhibitor, was used to determine the target site within SARS-CoV-2 PL^{pro}. The docking target site was determined by 3D structural alignment of SARS-CoV-2 PL^{pro} (PDB: 6W9C) with SARS-CoV PL^{pro} (PDB: 3MJ5). Hence, the grid box was generated by confining the essential residues lining this binding cavity. The three top hits were then re-docked individually using Autodock-Vina 1.1.2 to predict their binding modes and mechanism of interactions. The docking parameters were initially validated by redocking of native ligand GRL-0667S into the active site of SARS-CoV PL^{pro} (PDB: 3MJ5). Also, these hits were docked against SARS-CoV PL^{pro} (PDB: 3MJ5) and MERS-CoV PL^{pro} (PDB: 4R3D) using the same method. Discovery Studio Visualizer 4.5 [73] and PyMOL 1.3 [68] programs were used for data and interaction analyses.

2.4. In silico drug-likeness analysis and ADMET profiling

The available bioinformatics tool SwissADME (available online: http://www.swissadme.ch/index.php) [74] was used for finding the drug-likeness properties. Based on the Lipinski's rule of five [75], the properties that have been considered were molecular mass (MW), H-bond donor (HBD), H-bond acceptor (HBA), lipophilicity (log P), aqueous solubility and rotatable bonds (QP log S). PreADMET (https://preadmet.bmdrc.kr/) and pkCSM (http://biosig.unimelb.edu.au/pkcsm/) [76] servers were used to determine the ADMET (absorption, distribution, metabolism, excretion, and toxicity) parameters of candidate compounds.

2.5. MD simulation

All atoms MD simulation of SARS-CoV-2 PL^{pro}-inhibitor complexes and apo-protein were performed at 50 ns using GROMACS

2018 package [77]. The simulation was carried out using previously reported protocol [53,78]. Briefly, UCSF Chimera 1.14 was used to prepare the crystal structure of apo-SARS-CoV-2 PL^{pro} and in complex with the top pose of docked-compounds for MD simulation [79]. The topology and parameters of compounds were obtained using SwissParam (http://www.swissparam.ch/). The simulation was conducted by applying OPLS-AA/L force-field to the systems in a 3D cubic box of TIP3P model of water molecules. Next, the simulated systems were equilibrated, and energy minimized by steepest-decent algorithm, followed by equilibration using Canonical (NVT) as well as (isothermal/isobaric) NPT ensembles. The MD simulation was analyzed for the root-mean square deviation (RMSD), root-mean square fluctuations (RMSF), potential binding energy, a radius of gyration (Rg), H-bond interaction analysis, solvent accessible surface area (SASA) and principal component analysis (PCA).

2.6. Binding free-energy calculations

The binding free-energies (ΔG_{bind}) of the candidates were computed using the MM-PBSA algorithm [80], employed in AMBER 18, as previously described [81,82]. The molecular mechanics (MM) force fields were utilized to calculate the energy contributions of the receptor, ligand, and complex in a gaseous phase. The total binding free-energy (ΔG_{total}) is determined as a total energy released from the ligand/protein complex which is contributed by molecular mechanics binding energy (ΔE_{MM}) and solvation free energy (ΔG_{sol}) using the following equations:

$$\Delta E_{MM} = \Delta E_{int} + \Delta E_{ele} + \Delta E_{vdw}$$

$$\Delta G_{sol} = \Delta G_{pl} + \Delta G_{np}$$

$$\Delta G_{total} = \Delta E_{MM} + \Delta G_{sol}$$

$$\Delta G_{bind\ (MM\text{-}PB(GB)SA)} = \Delta E_{MM} + \Delta G_{sol} - T\Delta S$$

In which, ΔE_{MM} is divided into internal energy (ΔE_{int}), electrostatic energy (ΔE_{ele}), and van der Waals energy (ΔE_{vdw}), and the polar (ΔG_p) and non-polar (ΔG_{np}) energy components contributed to total solvation free energy (ΔG_{sol}). ΔG_{bind} is the free energy of binding evaluated after entropic calculations (-TΔS), for both MM-GBSA and MM-PBSA methods. In order to estimate the decisive role of interacting residues towards ligand's binding, per-residue energy decomposition analysis was performed using the MM-GBSA method, and binding energy was calculated as $\Delta G_{residue}$ using the following equation.

$$\Delta G_{residue} = \Delta E_{MM} + \Delta G_{sol}$$

The $\Delta G_{residue}$ includes the total energy obtained from sidechain and backbone energy decomposition. These methods have been well demonstrated in binding free energy calculations [83] for antiviral inhibitors [84,85].

3. Results and discussion

3.1. Sequence, structural and functional analysis of PL^{pro} for conserveness among coronaviruses

The sequence alignment of SARS-CoV-2 PL^{pro} displayed an identity of 82.80% and only 30.00% with SARS-CoV PL^{pro} and MERS-CoV PL^{pro}, respectively (Fig. 1). However, the sequence alignment revealed that PL^{pro} crucial catalytic triad residues of CoVs PL^{pro} were well conserved amongst SARS-CoV-2 (Cys111-His272-Asp286), SARS-CoV (Cys112-His273-Asp287) and MERS-CoV (Cys112-His275-Asp294).

In consistence with this, the structural alignment/superposition of all three human CoVs PL^{pro} revealed that the PL^{pro} of SARS-CoV-2 (Fig. 2A) adapted the same folding pattern as the PL^{pro} of SARS-CoV and MERS-CoV (Fig. 2B). Interestingly, the functionally well-conserved catalytic triad residues within the catalytic pockets of PL^{pro} among SARS-CoV-2, SARS-CoV, and MERS-CoV present at the identical place in the catalytic sites with RMSD 1.342 Å as presented in Figs. 2B and C. To determine the targetable binding site within the SARS-CoV-2 PL^{pro}, the crystal structure of SARS-CoV PL^{pro} in complex with a potent non-covalent inhibitor, GRL-0667S, was used for structural alignment. The binding site appeared as an allosteric site close to the active catalytic site (Figs. 2B and D).

3.2. Virtual screening of protease inhibitor library

The integrated computational method comprising virtual high throughput screening, molecular docking, and MD simulation is a significant approach for the exploration of potential inhibitors against a target protein [22,28,78,86]. In order to find out potential pan-PL^{pro} based anti-SARS-CoV-2 inhibitors, the structure-based screening was carried out against a virtual library of ~7,000 protease inhibitors. By applying a docking score cutoff of lower than −8.5 kcal/mol, three potential hits (Fig. 3) were selected with maximum scores, which were found to interact well with the active site residues. These include ADM_13083841 ((S)-4-(2-(2-(5-methyl-7-oxo-6,7-dihydropyrazolo [1,5-a]pyrimidin-2-yl)pyrrolidin-1-yl)-2-oxoethyl)phthalazin-1(2H) -one), AEM_16392818LMG_15521745 (N-(2-(3H-pyrazol-4-yl)ethyl) -4-((3-(2-fluorophenyl)isoxazol-5-yl)methyl)tetrahydro-2H-pyran-4-carboxamide) and SYN_15517940 ((R)-2-methyl-6-(((1R,5R)-8-oxo-1,5,6,8-tetrahydro-2H-1,5-methanopyrido[1,2-a] [1,5]diazocin-3(4H)-yl)sulfonyl)-2H-benzo[b] [1,4]oxazin-3(4H)-one), with binding energy score of −8.9, −8.7, −8.7 kcal/mol, respectively, and considered as potential inhibitors of SARS-CoV-2 PL^{pro} (Table 1). These three hit compounds were used to further evaluate the physiochemical and ADMET properties.

3.3. Analysis of screened inhibitor interaction

In order to understand the binding mode and mechanism of interaction of these compounds with SARS-CoV-2 PL^{pro}, an unbiased flexible docking of these compounds into the active site of the SARS-CoV-2 PL^{pro} enzyme was performed. The docking and scoring functions had been validated before the docking was carried out. Since SARS-CoV and SARS-CoV-2 shared significant sequence similarity and similar 3D structure, the validation was achieved by docking the GRL-0667S, a potent SARS CoV PL^{pro} inhibitor with an IC_{50} value of 0.32 ± 0.01 μM, into the same site within SARS-CoV-2 [87]. The latter approach was made to evaluate the ability of the docking protocol to predict the biologically active conformation. Moreover, as shown in Fig. 4, both the docked conformation within SARS-CoV-2 and co-crystal ligand within SARS-CoV adapted a similar binding mode within the target site, validating the robustness of the docking protocol.

Flexible docking revealed that the three compounds adopted the same binding mode within the binding pocket and interacted through H-bonds as shown in Fig. 5. Among the conserved H-bonds interactions, the terminal pyrimidin-4-one of ADM_13083841, central oxane moiety of LMG_15521745 and terminal benzoxazines moiety of SYN_15517940 established one H-bond each with the side chain oxygen atom of Thr301. The second conserved H-bond was established between the side chain oxygen of Tyr264 and the central pyrrolidine moiety of ADM_13083841, oxazole moiety of LMG_15521745, and sulfonamide moiety of SYN_15517940. Apart

```
4R3D:B|MERS-CoV     GPLGSQQLTIEVLVTVDGVNFRTVVLNNKNTYRSQLGCVFFNGADISDTIPDEKQNGHSL    60
6W9C:A|SARS-CoV-2   -----EVRTIKVFTTVDNINLHTQVVDMSMTYGQQFGPTYLDGADVTKIKPHNSHEGKTF    55
3MJ5:A|SARS-CoV     ----MEVKTIKVFTTVDNTNLHTQLVDMSMTYGQQFGPTYLDGADVTKIKPHVNHEGKTF    56
                         :  **:*:.***. *::* ::: . ** .*:* .:::***::.  *. .::*:::

4R3D:B|MERS-CoV     YLADNLTADETKALKELYGPVDPTFLHRFYSLKAAVHKWKMVVCDKVRSLKLSDNNCYLN   120
6W9C:A|SARS-CoV-2   YVLPNDDTLRV-EAFEYYHTTDPSFLGRYMSALNHTKKWKYPQVNGLTSIKWADNNCYLA   114
3MJ5:A|SARS-CoV     FVLPSDDTLRS-EAFEYYHTLDESFLGRYMSALNHTKKWKFPQVGGLTSIKWADNNCYLS   115
                    ::  .  : .     * *   * :** *: *    .:***    . : *:* :******

4R3D:B|MERS-CoV     AVIMTLDLLKDIKFVIPALQHAFMKHKGGDSTDFIALIMAYGNCTFGAPDDASRLLHTVL   180
6W9C:A|SARS-CoV-2   TALLTLQQI-ELKFNPPALQDAYYRARAGEAANFCALILAYCNKTVGELGDVRETMSYLF   173
3MJ5:A|SARS-CoV     SVLLALQQL-EVKFNAPALQEAYYRARAGDAANFCALILAYSNKTVGELGDVRETMTHLL   174
                    :.:::*: : ::**  ****.*: : :.*::::* ***:** * *.*  .*. . :  ::

4R3D:B|MERS-CoV     AKAELCCSARMVWREWCNVCGIKDVVLQGLKACCYVGVQTVEDLRARMTYVCQCGGERHR   240
6W9C:A|SARS-CoV-2   QHANLD-SCKRVLNVVCKTCGQQQTTLKGVEAVMYMGTLSYEQFKKGVQIPCTCGKQATK   232
3MJ5:A|SARS-CoV     QHANLE-SAKRVLNVVCKHCGQKTTTLTGVEAVMYMGTLSYDNLKTGVSIPCVCGRDATQ   233
                     :*:*  *.: * .  *: ** : ..* *::*  *:*. : ::::  :   * ** :  :

4R3D:B|MERS-CoV     QIVEHTTPWLLLSGTPNEKLVTTSTAPDFVAFNVFQGIETAVGHYVHARLKGGLILKFDS   300
6W9C:A|SARS-CoV-2   YLVQQESPFVMMSAPPAQYELKHGT---FTCASEYTG-NYQCGHYKHITSKET-LYCIDG   287
3MJ5:A|SARS-CoV     YLVQQESSFVMMSAPPAEYKLQQGT---FLCANEYTG-NYQCGHYTHITAKET-LYRIDG   288
                     :*:: : ::::*. * :  :  .*   * . . : * :   *** *   *   :  :*.

4R3D:B|MERS-CoV     GTVSKTSDWKCKVTDVLFPGQKYSSDCNVVRYSLDG     336
6W9C:A|SARS-CoV-2   ALLTKSSEYKGPITDVFYKENSYTTTIKAA------     317
3MJ5:A|SARS-CoV     AHLTKMSEYKGPVTDVFYKETSYTTTIK--------     316
                    . ::* *::*  :***::   .*::  :
```

Fig. 1. Multiple sequence alignments of SARS-CoV-2 PL^{pro} with SRAS-CoV PL^{pro} and MERS-CoV PL^{pro}. The conserved catalytic triad residues (Cys111-His272-Asp286) within SARS-CoV-2, (Cys112-His273-Asp287) within SARS-CoV, and (Cys112-His275-Asp294) within MERS-CoV are highlighted with red color arrows.

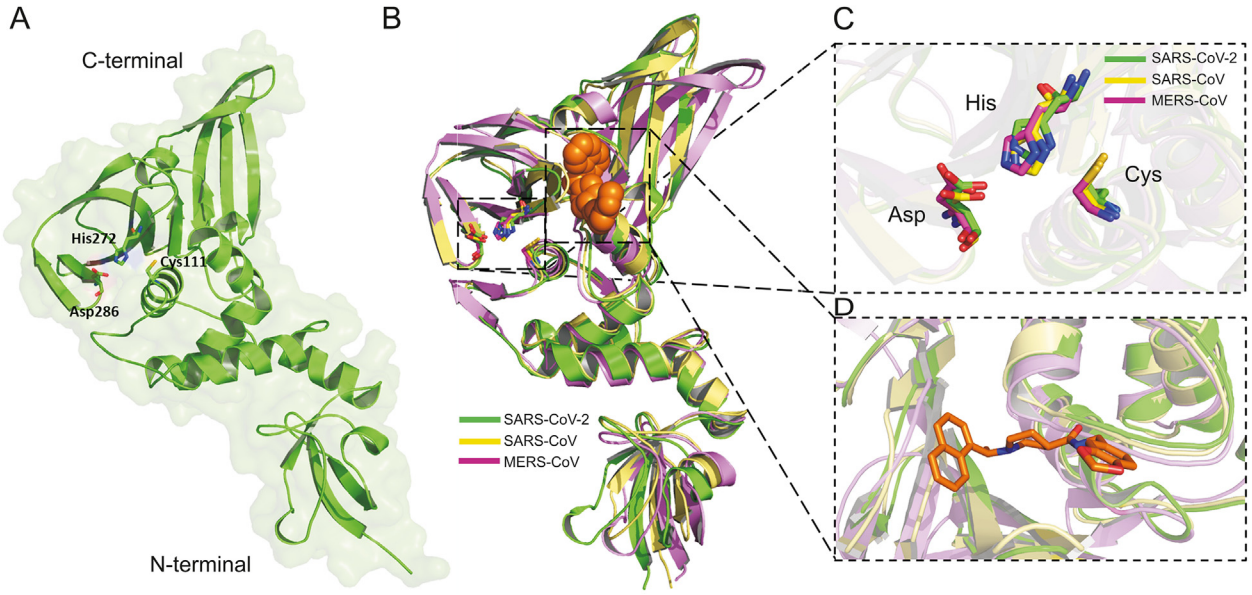

Fig. 2. (A) The 3D structures of SARS-CoV-2 PL^{pro} enzymes. The catalytic triad residues Cys111-His272-Asp286 were shown green sticks. (B) The overlapping of the 3D structures of PL^{pro} enzymes of SARS-CoV-2 (green) (PDB: 6W9C), SRAR-CoV (yellow) (PDB: 3MJ5) and MERS-CoV (purple) (PDB: 4R3D). The conserved catalytic triad residues with each structure were shown in sticks. GRL-0667S within the binding site of SRAS-CoV PL^{pro} was shown in orange spheres. (C) The overlapping of the catalytic triad residues of PL^{pro} within the active sites of SARS-CoV-2 (green sticks), SRAR-CoV (cyan sticks), and MERS-CoV (pink sticks). (D) Close view to the targetable binding pocket within PL^{pro} enzyme based on the binding mode of GRL-0667S with SARS-CoV PL^{pro}.

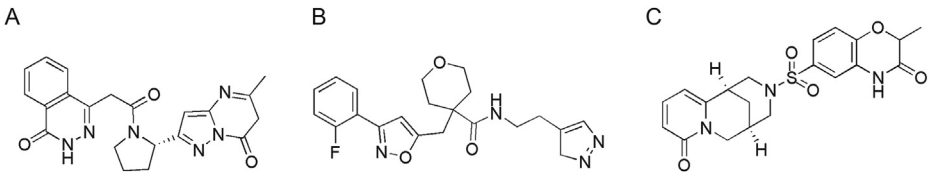

Fig. 3. Chemical structures of screened hits; (A) ADM_13083841, (B) LMG_15521745 and (C) SYN_15517940.

Table 1
Properties profile of candidate compounds.

Name (ID)	Binding score (kcal/mol)	Hydrogen bond interaction	Hydrophobic interaction
ADM_13083841	−8.9	Lys157, Tyr264, Thr301	Leu162, Met208
LMG_15521745	−8.7	Lys157, Tyr264, Thr301	Leu162, Pro248
SYN_15517940	−8.7	Arg166, Thr264, Thr301	Leu162, Met208, Pro248

from these, ADM_13083841 and LMG_15521745 also established conserved interactions with the side-chain nitrogen (N) of Lys157, while SYN_15517940 established H-bond with the side-chain N of Arg166. Moreover, these compounds also formed a conserved network of hydrophobic interactions with the surrounding residues, including Leu162, Asp164, Met208, Pro247, Pro248, and Tyr268. The molecular interaction analyses were found in agreement with the co-crystallized inhibitors of SARS-CoV-PL^{pro} (PDB ID: 3E9S and 3MJ5) [87] (Table 1).

3.4. ADMET screening and drug-ability results

ADMET-based drug scan tool at the SwissADME server was used to evaluate the drug-likeness of the proposed SARS-CoV-2 PL^{pro} inhibitors [74]. ADM_13083841 ($C_{21}H_{20}N_6O_3$) is a phthalazinone derivative with the log P value of 2.04 and molecular weight of 404.42 g/mol. The compound has six hydrogen-bond acceptor (HBA) and one hydrogen-bond donor (HBD) atoms. Another oxazole based compound selected from the docked molecules is LMG_15521745 ($C_{21}H_{23}FN_4O_3$) with the log P value of 3.02 and molecular weight of 398.43 g/mol. It contains seven HBA atoms and one HBD. SYN_15517940 ($C_{20}H_{21}N_3O_5S$) has a log P value of 2.30 and a molecular weight of 415.46 g/mol, together with six HBA atoms and one HBD (Table 2).

For further validation of the drug likeliness capability of target compounds, all these compounds were subjected to the PreADMET and pkCSM servers, which have five main parameters (absorption, distribution, metabolism, excretion, and toxicity) for assessment. These five parameters were then assessed according to the number of thresholds. All the three compounds successfully passed the criteria of drug-ability (Table 3).

3.5. MD simulation

MD simulation is a widely used computational method to analyze the dynamic behavior and stability of a ligand/protein complex under different conditions [30,53,88,89]. All atoms MD simulations were carried out on the initial conformation of the hit compounds-PL^{pro} complexes obtained after the docking in the solvated states at 50 ns.

3.5.1. RMSD, RMSF and potential binding energy

The RMSD computes the direct changes in the atoms of superimposed proteins and is an acceptable approach to assess the stability of protein/ligand complexes [90–93]. The RMSD values of the Cα-backbone atoms of SARS-CoV-2 PL^{pro} in complex to the three PL^{pro} potential inhibitors were calculated with respect to the initial structure and compared with apo-protein in an unbound form. The RMSD values steadily increased in the beginning and remained converged throughout the simulation period, especially for ADM_13083841 and LMG_15521745 complexes. Similarly, the RMSD values of apo-protein reached an equilibrium after an initial

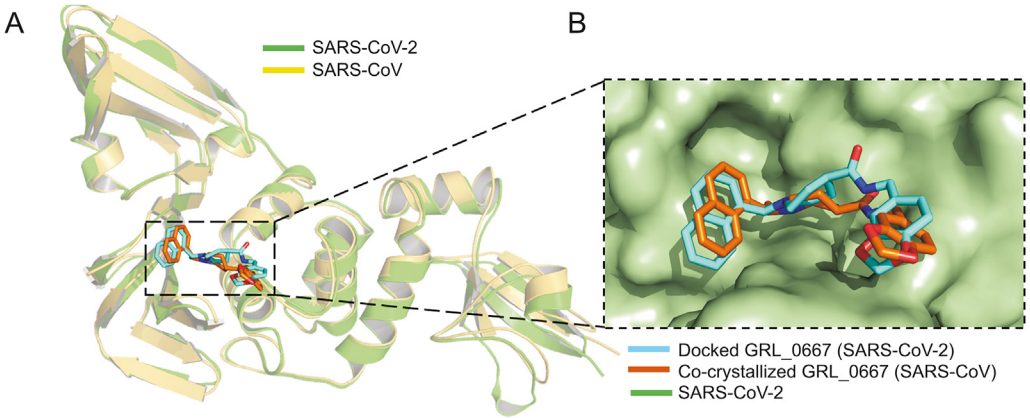

Fig. 4. Validation of the docking protocol. (A) Ribbon representation for superimposition of docked GRL-0667S (cyan) into SARS-CoV-2 PL^{pro} (green) (PDB: 6W9C), and co-crystalized structure (orange) of GRL-0667S within the active site of SARS CoV PL^{pro} (yellow) (PDB: 3MJ5). (B) Superimposition of co-crystallized (orange) and best-docked pose (cyan) of inhibitor GRL-0667S in the active site of SARS-CoV-2 PL^{pro} (PDB ID: 6W9C, green molecular surface).

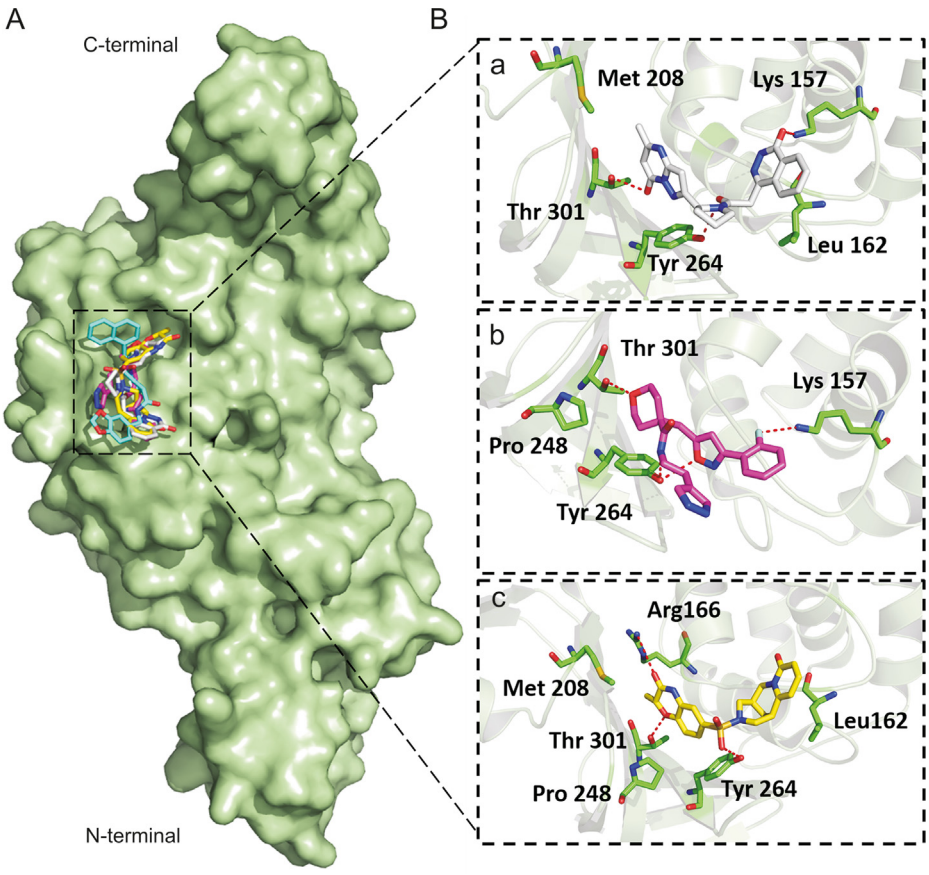

Fig. 5. Binding modes and molecular interactions of screened compounds with SARS-CoV-2 PL^{pro} (PDB: 6W9C). (A) Surface representation of the binding mode of GRL-0667S (cyan), ADM_13083841 (white), LMG_15521745 (pink) and SYN_15517940 (yellow) to SARS-CoV-2 PL^{pro} (green). (B) The mechanism of molecular interactions of (a) ADM_13083841 (white), (b) LMG_15521745 (pink) and (c) SYN_15517940 (yellow) to SARS-CoV-2 PL^{pro} (green).

increase within the first 5 ns and converged between 0.12 and 0.3 nm throughout the simulation course. The average RMSD values for the last 45 ns for apo-protein, ADM_13083841, LMG_15521745, and SYN_15517940 complexes were 0.18 ± 0.03, 0.18 ± 0.03, 0.19 ± 0.04 and 0.18 ± 0.03 nm, respectively (Fig. 6A).

The RMSF measured the local protein flexibility and proved to be an excellent parameter to investigate the protein's residual flexibility over the simulation period [90,92]. The time average of protein backbone RMSF values of the 315 amino acids of SARS-CoV-2 PL^{pro} protein with and without the three candidate compounds was calculated over the 50 ns simulation period. Normal fluctuations in the constituent residues of SARS-CoV-2 PL^{pro} were observed for apo-protein and all three complexes, PL^{pro}-ADM_13083841, PL^{pro}- LMG_15521745 and PL^{pro}- SYN_15517940, and were plotted to compare the residual flexibility. As shown in Fig. 6B, major fluctuations were observed mainly in the loop regions (residue nos. 185–200 and 220–230), located away from the binding pocket. The average RMSF values were calculated as 0.09 ± 0.05, 0.11 ± 0.05, 0.11 ± 0.06 and 0.09 ± 0.04 nm for apo-protein, ADM_13083841, LMG_15521745 and SYN_15517940, respectively.

Furthermore, the potential energy over the simulation time for the three complexes and apo-protein was calculated. The results indicated that the three complexes remained in a stable pattern throughout the 50 ns simulations, as shown in Fig. 6C. These RMSD, RMSF, and potential energy MD simulation results confirmed the stability of all selected compounds at the catalytic-site of SARS-CoV-2 PL^{pro}.

Table 2
Drug-likeness properties of identified compounds.

Name	MW (g/mol)	HBD	HBA	Log P	RB	Log S
ADM_13083841	404.42	1	6	2.04	4	−2.84 Soluble
LMG_15521745	398.43	1	7	3.02	8	−3.54 Soluble
SYN_15517940	415.46	1	6	2.30	2	−2.62 Soluble

MW: molecular weight.

3.5.2. Rg, hydrogen bond interaction and SASA analysis

The Rg is a parameter for evaluating the behavior and stability of the biological systems during the MD trajectories by measuring the compactness of biomacromolecules' structures [94,95]. The Rg can also be used as an indicator of whether the complex will maintain folded conformation after the MD simulation. The Rg values of the three complexes and apo-protein were stabilized after the initial increase at 5 ns, supporting the RMSD results that systems had reached the equilibrium state (Fig. 7A). The average Rg values for the three complexes and apo-protein remained relatively consistent for the last 45 ns, indicating a stably folded structure with an average value of 2.32 ± 0.01, 2.32 ± 0.02, 2.32 ± 0.02 and 2.31 ± 0.01 nm for apo-protein, ADM_13083841, LMG_15521745, and SYN_15517940, respectively.

Hydrogen bonds play a crucial role as stabilizing forces for a ligand-protein complex [90–92]. The total number of hydrogen bonds formed between the three candidate compounds and SARS-CoV-2 PL^{pro} is shown in Fig. 7B. All candidate compounds can make

Table 3
ADMET profiling for absorption, metabolism and toxicity parameters of identified compounds.

Model	ADM_13083841	LMG_15521745	SYN_15517940
Absorption and distribution			
Blood-brain barrier	No	No	No
Human intestinal absorption	High	High	High
Caco-2 permeability	Yes	Yes	No
P-glycoprotein inhibitor	Substrate/inhibitor	Non-substrate/inhibitor	Non-substrate/non-inhibitor
Organic cation transporter 2 (OTC2)	Non-inhibitor	Non-inhibitor	Non-inhibitor
Metabolism			
CYP450 2C9	Non-inhibitor	Inhibitor	Non-inhibitor
CYP450 2D6	Non-substrate/non-inhibitor	Non-substrate/non-inhibitor	Non-substrate/non-inhibitor
CYP450 3A4	Substrate/non-inhibitor	Substrate/inhibitor	Substrate/non-inhibitor
CYP450 1A2	Non-inhibitor	Non-inhibitor	Non-inhibitor
CYP450 2C19	Inhibitor	Inhibitor	Non-inhibitor
Toxicity			
Acute algae toxicity	0.0264273	0.0621567	0.158197
Ames test	Mutagen	Mutagen	Non-mutagen
Carcinogenicity (Mouse)	Negative	Negative	Negative
Carcinogenicity (Rat)	Negative	Negative	Negative
Acute daphina toxicity	0.12599	0.364329	0.661198
In vitro hERG inhibition	High risk	High risk	Medium risk
Acute fish toxicity (medaka)	0.0354928	0.227324	0.836634
Acute fish toxicity (minnow)	0.0544461	0.248798	0.94807
Ames TA100 (+S9)	Positive	Negative	Negative
Ames TA100 (-S9)	Negative	Negative	Negative
Ames TA1535 (+S9)	Negative	Positive	Negative
Ames TA1535 (-S9)	Negative	Positive	Negative

up to four stable hydrogen bonds with SARS-CoV-2 PL^{pro} throughout the simulation period supporting the docking results. These bonding parameters represented that all candidate compounds may bind effectively and tightly to the SARS-CoV-2 PL^{pro}.

The SASA is a tool to measure the water accessible proportion of the biomolecule surface [96]. The calculation of SASA value is a useful tool to predict the degree of the conformational changes which resulted due to complex interaction. The calculated average SASA values for the last 45 ns simulation time were 165.27 ± 1.22, 164.78 ± 1.21, 165.18 ± 1.18, and 165.51 ± 1.27 nm^2, respectively (Fig. 7C). These results suggested there were no observed changes in the accessibility area of all three systems over the 50 ns simulation time. Thus, in terms of SASA analysis, the relative stability of our protein-ligand complexes has been concluded.

3.5.3. PCA

The PCA analysis was performed to identify conformational changes that accompanied the ligands binding within different protein/ligand complexes. In the current study, the first two principal components (PC1 and PC2) were selected for predicting the protein motions. The projection of two eigenvectors for apo-protein as well as all three complexes, PL^{pro}-ADM_13083841, PL^{pro}-LMG_15521745, and PL^{pro}-SYN_15517940 is shown (Fig. 8). Generally, the complex that occupies a more phase-space with a non-stable cluster and complex that occupies less phase-space with a stable cluster represented a less stable complex and a more stable complex, respectively. From the graphs, the apo-protein, as well as the three complexes, occupied less phase-space. The clusters shifting were from −4 to 5 nm in case of apo-protein, −8 to 6 nm in case of ADM_13083841. In contrast, the clusters shifting were from −6 to 6 and −4 to 4 in cases of LMG_15521745 and SYN_15517940, respectively. With respect to apo-protein values, all complexes showed a very stable complex.

3.6. Predicted binding free energy calculations

The MM/GBSA and MM/PBSA are both end-point methods and present more physically meaningful information than docking scoring functions. These methods have been extensively utilized in the identification of potential antiviral inhibitors [83,84,97,98]. The absolute energy of binding (ΔG_{bind}) of all three hit compounds together with co-crystallized PL^{pro} inhibitor, GRL-0667S [87], was predicted through mechanics/Poisson–Boltzmann (generalized born) surface area (MM/PB(GB)SA) method on 50 snapshots extracted from the last 20 ns of the simulation period. It is important to note that we also incorporated entropic contributions (-TΔS) in ligand binding, which are computationally expensive in the MMPBSA method and give better accuracy [99]. Moreover, entropy effects play an essential role in protein-ligand interactions [100]. The calculations are tabulated in Table 4.

According to the MM/PB(GB)SA calculations, van der Waals (ΔE_{vdW}) interaction was the main driving force in complex stabilization with ADM_13083841 (ΔE_{vdW} = −46.12 kcal/mol), LMG_15521745 (ΔE_{vdW} = −41.3 kcal/mol) and SYN_15517940 (ΔE_{vdW} = −39.88 kcal/mol), and was about 1–2 fold stronger than electrostatic attraction energy (ΔE_{ele}) predicted to be −14.1, −16.24, and 15.3 kcal/mol, respectively. Therefore, it was found that compounds interacted mainly through van der Waals interactions and these findings are in agreement with the co-crystalized GRL-0667S (ΔE_{vdW} = −43.7 and ΔE_{MM} = −12.39) [87]. Together with the solvation effect in ADM_13083841 ($\Delta G_{sol(PBSA)}$ = 30.83; $\Delta G_{sol(GBSA)}$ = 24.03 kcal/mol), LMG_15521745 ($\Delta G_{sol(PBSA)}$ = 32.15; $\Delta G_{sol(GBSA)}$ = 25.48 kcal/mol) and SYN_15517940 ($\Delta G_{sol(PBSA)}$ = 26.17; $\Delta G_{sol(GBSA)}$ = 20.32 kcal/mol) complexed with SARS-COV-2 PL^{pro} and incorporation of entropic terms, the absolute ΔG_{bind} accounted for −5.09 (ADM_13083841), −4.17 (LMG_15521745) and −7.11 kcal/mol (SYN_15517940) as per MM-PBSA ($\Delta G_{bind(MM/PBSA)}$) approach and values of 11.89 (ADM_13083841), −10.84 (LMG_15521745) and −12.96 kcal/mol (SYN_15517940) were taken from the MM-PBSA ($\Delta G_{bind(MM/PBSA)}$) approach. The obtained ΔG_{bind} values of all three compounds were in agreement with the co-crystalized GRL-0667S, which revealed relatively similar values by MM/PBSA (−5.81 kcal/mol) and MM/GBSA (−9.82 kcal/mol) methods.

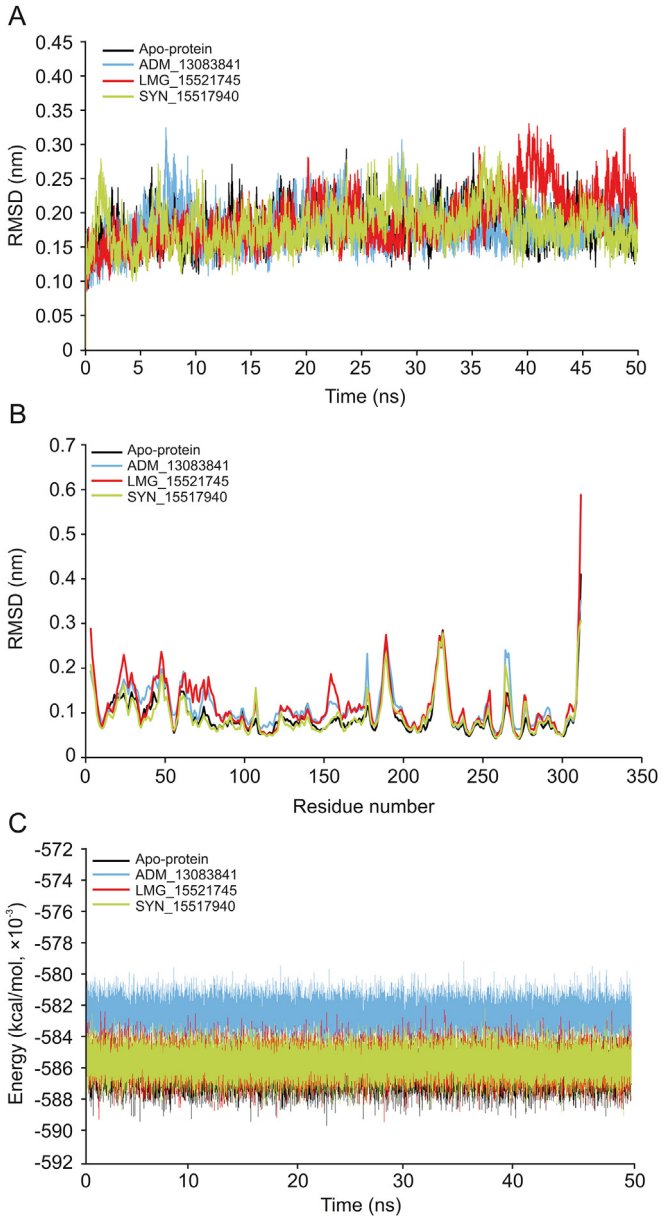

Fig. 6. (A) The root mean square deviation (RMSD) of C–Cα–N backbone vs. simulation time for solvated SARS-CoV-2 PL^{pro} in apo-state and in complex with the three candidate compounds over the time of 50 ns MD simulation. (B) The root mean square fluctuation (RMSF) of SARS-CoV-2 PL^{pro} in apo-state and in complex with the three candidate compounds. (C) The potential energy for SARS-CoV-2 PL^{pro} in apo-state and in complex with the candidate compounds over the time of 50 ns MD simulation.

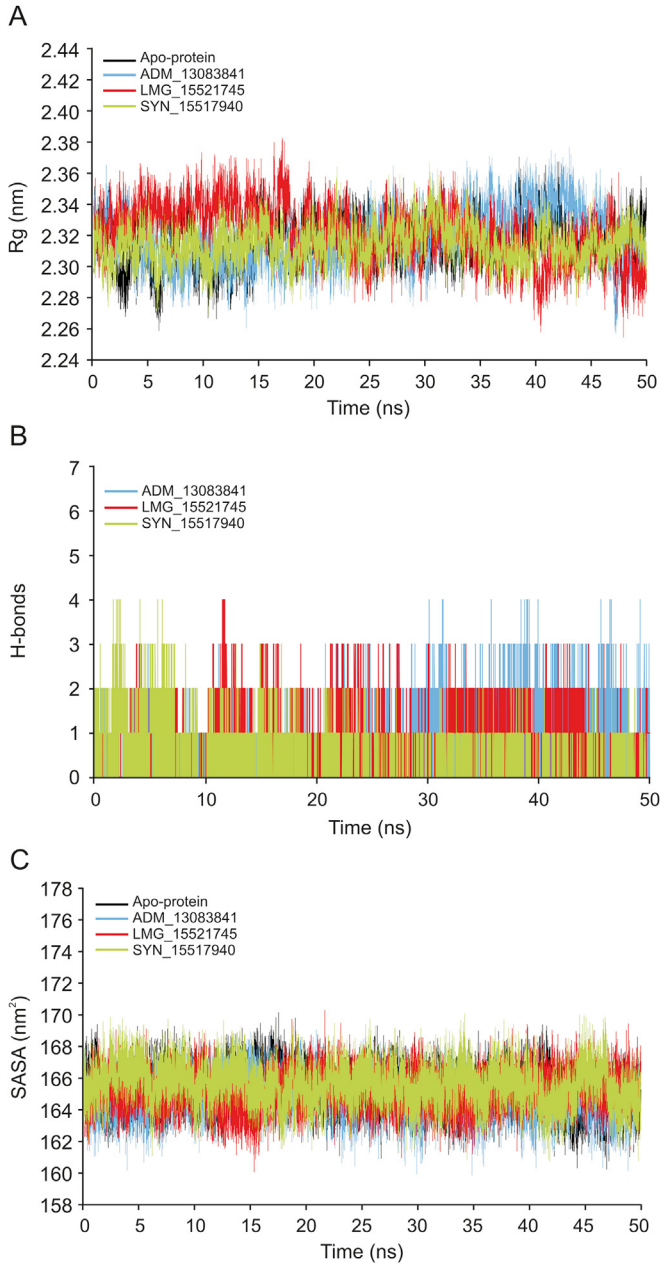

Fig. 7. (A) The radius of gyration (Rg) of SARS-CoV-2 PL^{pro} in apo-state and in complex with the three candidate compounds during 50 ns MD simulation. (B) Plot of number of hydrogen bond within the SARS-CoV-2 PL^{pro} in complex with the three candidate compounds during 50 ns MD simulation. (C) Plot of solvent accessible surface area (SASA) of SARS-CoV-2 PL^{pro} in apo-state and in complex with the three candidate compounds over the time of 50 ns MD simulation.

3.6.1. Per-residue decomposition analysis

In order to evaluate the binding role of key interacting residues of the active site, ($\Delta G_{residue}$) calculations were performed using the MMGBSA method. The total energy decomposition values associated with ligand binding is presented in Fig. 9. We highlight here only the significant energy contributing residues in ligand binding. Briefly, the obtained results revealed that residues, including Asp164, Met208, Pro247, Pro248, Tyr264 and Thr301 located in the active site of SARS-COV-2 PL^{pro}, were found important for interactions with ADM_13083841, LMG_15521745, and SYN_15517940. Among these, the residual decomposition analysis revealed the favorable contributions (<−1.7 kcal/mol) of Asp164, which exhibited $\Delta G_{residue}$ of −1.92, −1.86, and −1.74 kcal/mol, Tyr264 which exhibited $\Delta G_{residue}$ of −2.14, −2.08, and −2.81 kcal/mol with ADM_13083841, LMG_15521745 and SYN_15517940, respectively. Moreover, Tyr264 was also found interacting through H-bonds in all three complexes (Fig. 5).

In comparison, the $\Delta G_{residue}$ values of co-crystallized GRL-0667S showed a relatively similar trend. Hence, $\Delta G_{residue}$ energies of highly interacting residues suggested that the molecular structures of all three compounds fitted well inside the active-site of SARS-COV-2 PL^{pro}. Moreover, the obtained results after residual decomposition analysis were in accordance with the complex stability analysis through MD simulation, where the stable RMSD was achieved due to these pairwise interactions throughout the simulation

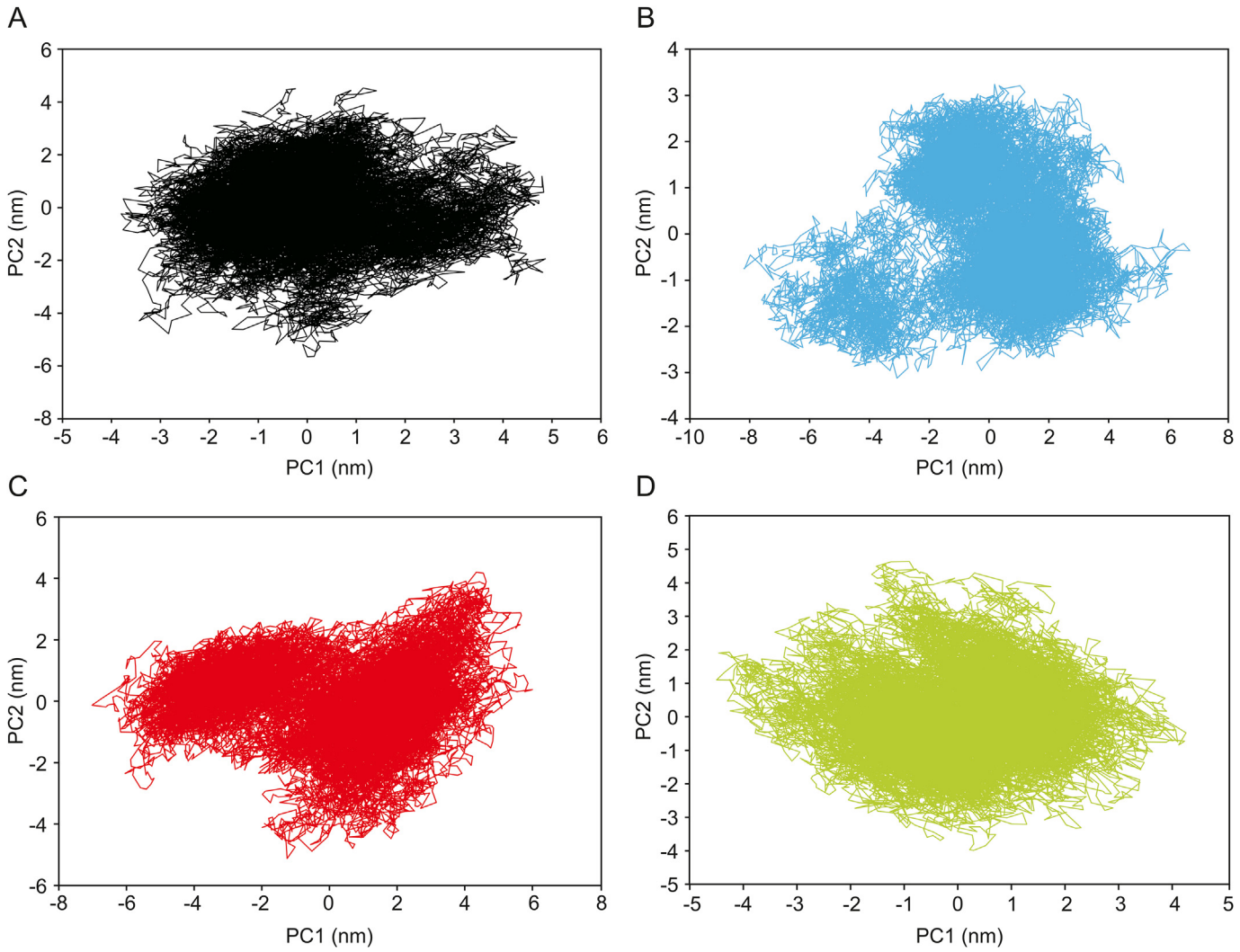

Fig. 8. Two-dimensional principle component analysis (PCA) projections of trajectories obtained from 50 ns MD simulations. (A) Apo-protein, (B) ADM_13083841, (C) LMG_15521745, and (D) SYN_15517940.

Table 4
ΔG_{bind} values of ADM_13083841, LMG_15521745 and SYN_15517940 in complex with SARS-CoV-2 PL^{pro} calculated by the MM/PB(GB)SA method.

Energy component	ADM_13083841	LMG_15521745	SYN_15517940	GRL-0667S
MM (gas term)				
ΔE_{vdw}	−46.12	−41.3	−39.88	−43.7
ΔE_{ele}	−14.1	−16.24	−15.3	−12.39
ΔE_{MM}	−60.22	−57.54	−55.18	−56.09
(−)TΔS	24.3	21.22	21.9	20.91
PBSA (solvation term)				
$\Delta G_{p(PBSA)}$	35.9	37.26	31.27	34.76
$\Delta G_{np(PBSA)}$	−5.07	−5.11	−5.1	−5.39
$\Delta G_{sol(PBSA)}$	30.83	32.15	26.17	29.37
GBSA (solvation term)				
$\Delta G_{p(GBSA)}$	29.45	31.37	27.23	31.38
$\Delta G_{np(GBSA)}$	−5.42	−5.89	−6.91	−6.02
$\Delta G_{sol(GBSA)}$	24.03	25.48	20.32	25.36
Binding free energy				
$\Delta G_{bind(MM/PBSA)}$	−5.09	−4.17	−7.11	−5.81
$\Delta G_{bind(MM/GBSA)}$	−11.89	−10.84	−12.96	−9.82

Note: The co-crystalized complex GRL-0667S/SARS-CoV-2 PL^{pro} (PDB: 3MJ5) was used as positive control. ΔG_{bind} is the sum of molecular mechanics energy (ΔE_{MM}) which is the gas term, and solvation free energy (ΔG_{sol}). Both ΔE_{MM} and ΔG_{sol} are further divided into internal energy (ΔE_{int}), electrostatic energy (ΔE_{ele}), and van der Waals (ΔE_{vdw}) energy, and polar (ΔG_p) and non-polar (ΔG_{np}) contributions to the solvation free energy. Solvation term were included from both MM/PBSA and MM/GBSA methods. These calculations were executed with the incorporation of entropic term (TΔS) by the following equation: $\Delta G_{bind\ (MM\text{-}PB(GB)SA)} = \Delta E_{MM} + \Delta G_{sol} - T\Delta S$.

period. Hence, we hypothesized that these critically important active site residues might be crucial in inhibitor recognition for the development of SARS-COV-2 PL^{pro} inhibitors and could lead to further optimization of these compounds.

3.7. Molecular docking of screened hits with SARS-CoV and MERS-CoV PL^{pros}

Disulfiram is an FDA approved drug used to treat chronic alcoholism. Previous research reported that disulfiram can inhibit SARS-CoV and MERS-CoV PL^{pros} as an allosteric, competitive or mixed inhibitor [101]. Disulfiram has also been proposed for the treatment of SARS-CoV-2 [102–104]. Similarly, previous studies reported that lopinavir showed promising results against MERS-CoV [105–108] and SARS-CoV [109–111], and currently it is under clinical trials for COVID-19 treatment [11,112–114]. Lopinavir is an FDA approved serine protease inhibitor used to treat HIV-1 infection [115]. Therefore, to test the hypothesis and validate the possibility of pan-PL^{pro} based broad-spectrum inhibitors, next we determined the ability of the selected compounds to bind to the SARS-CoV and MERS-CoV PL^{pros}, by the validated flexible docking approach into the same target site. Interestingly, these compounds showed high binding affinity toward SARS-CoV PL^{pro} with binding energy scores ranged from −8.7 to −7.9 kcal/mol (Fig. 10). However, the binding energy scores of these compounds were low in the case of MERS-CoV, ranging from −5.9 to −6.7 kcal/mol, indicating that their activity toward SARS-CoV might be greater than the activity against MERS-CoV (Fig. 11). This could be due to the structural difference of MERS-CoV blocking loop 2 [116].

Our effort to target the deadliest human CoVs (SARS-CoV, SARS-CoV-2 and MERS-CoV) PL^{pro} concurrently by investigating their conservation (structural and functional) produced significant results. The present study identified three small-molecule protease inhibitors with great capability of drug leads, capable of inhibiting

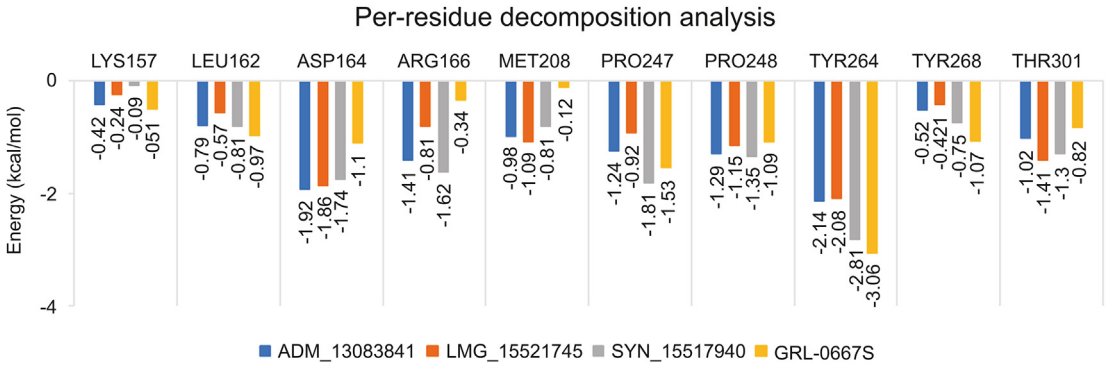

Fig. 9. Per-residue decomposition analysis using MM-GBSA methods and highly interacting binding site residues are displayed together with $\Delta G_{residue}$ derived from last 20 ns of MD simulations.

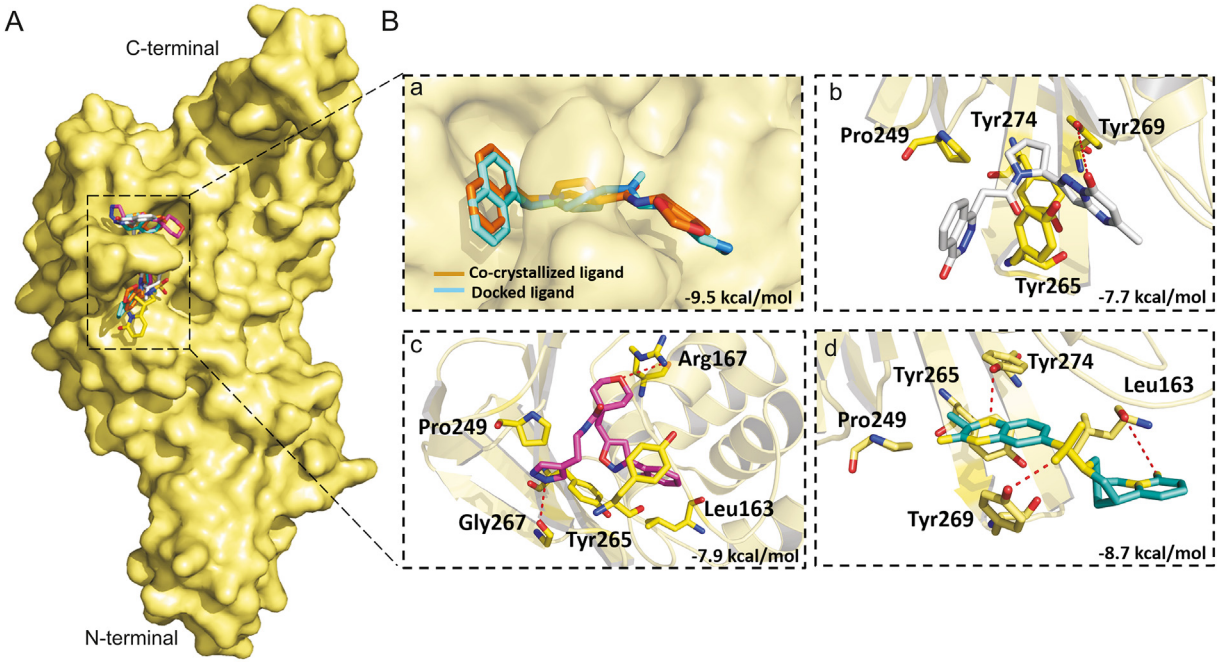

Fig. 10. Binding modes and molecular interactions of screened compounds with SARS-CoV PL^{pro} (PDB: 3MJ5). (A) Surface representation of the binding mode of co-crystalized GRL-0667S (cyan), docked GRL-0667S (orange), ADM_13083841 (white), LMG_15521745 (pink) and SYN_15517940 (green) to SARS-CoV PL^{pro} (yellow). (B) The mechanism of molecular interactions of compounds to SARS-CoV PL^{pro}. Close view to the binding mode of (a) co-crystalized GRL-0667S (cyan) and docked GRL-0667S (orange) to SARS-CoV PL^{pro}, (b) ADM_13083841 (white), (c) LMG_15521745 (pink) and (d) SYN_15517940 (green) to SARS-CoV-2 PL^{pro}.

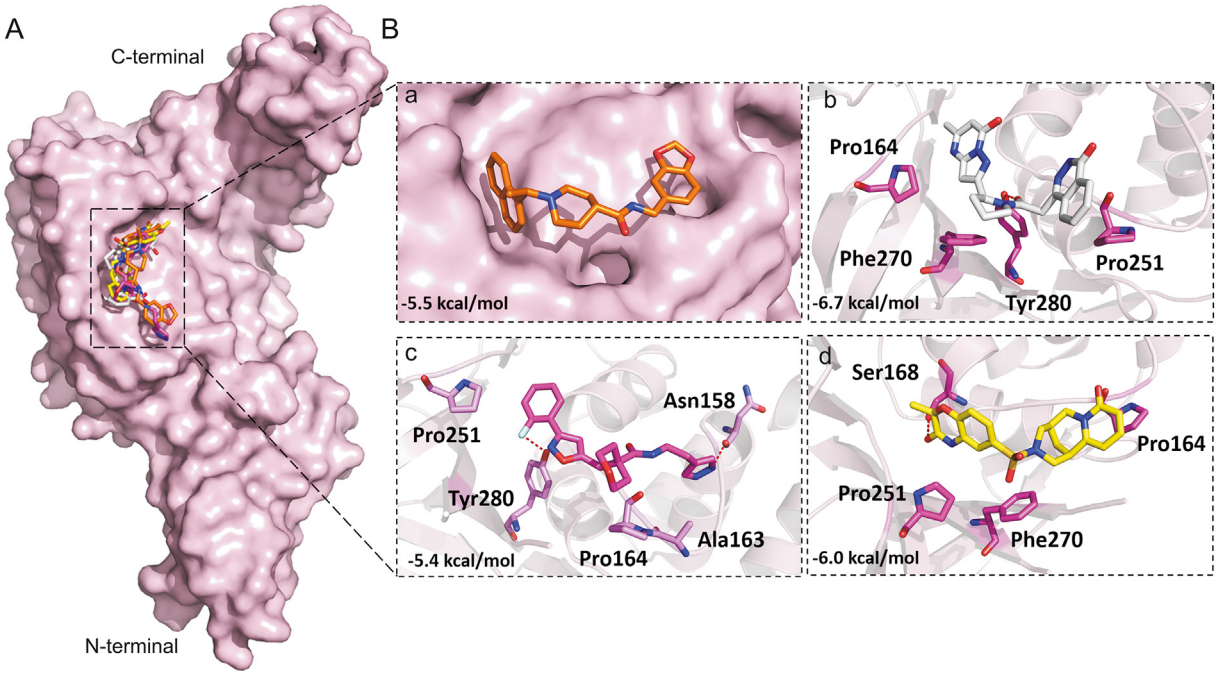

Fig. 11. Binding modes and molecular interactions of screened compounds with MERS-CoV PL^{pro} (PDB: 4R3D). (A) Surface representation of the binding mode of docked GRL-0667S (orange), ADM_13083841 (white), LMG_15521745 (pink) and SYN_15517940 (yellow) to MERS-CoV PL^{pro} (pink). (B) The mechanism of molecular interactions of compounds to MERS-CoV PL^{pro}. Close view to the binding mode of (a) docked GRL-0667S (orange), (b) ADM_13083841 (white), (c) LMG_15521745 (pink) and (d) SYN_15517940 (green) to MERS-CoV PL^{pro}.

PL^{pro} of SARS-CoV-2. These set of compounds could function as broad-spectrum pan-PL^{pro} inhibitors against deadly human CoVs infections. This is critically important against constantly evolving CoVs. The benefits of treatment strategies involving pan-inhibitors have already been reported in the case of Dengue virus [28,117], HCV [118–121], and HIV [122]. The screened inhibitors in the present study may lead towards a medicinal solution against the variety of constantly evolving CoVs by effectively targeting/hindering the proteolytic role of their PL^{pros}. Therefore, our findings warrant further experimental work on screened pan-PL^{pro} inhibitors for further drug optimization.

4. Conclusions

This comprehensive study offers an integrated computational approach towards the discovery of three novel hit compounds, screened from a focused library of ~7,000 compounds having a diverse scaffold that can specifically target SARS-COV-2 PL^{pro}, which permits in vitro evaluations. These three compounds, ADM_13083841, LMG_15521745, and SYN_15517940, were selected for further computational studies to gain a deep insight into their binding mode, mechanism of molecular interaction, and ADMET analysis. The in-depth structural exploitation of key residues of the active site together with the dynamic scaffolds of hit compounds adopted after 50 ns MD simulations offered the way to design broad-spectrum inhibitors against deadly human CoVs. The structural/functional conservation of SARS-CoV, MERS-CoV, and SARS-CoV-2 revealed strikingly similar conformations of active site residues. Altogether, the identification of highly contributing residues towards overall ligand binding energy might provide an excellent platform to further enhance the inhibitor recognition potential of SARS-COV-2 PL^{pro}. Although the present study lacks in silico binding mode validation, the structural evidence obtained from this computational study has surfaced the way in the designing of pan-PL^{pro} based inhibitors as broad-spectrum antiviral agents to combat SARS-CoV-2 and other pathogenic human coronaviruses.

Declaration of competing interest

The authors declare that there are no conflicts of interest.

Acknowledgments

This work was supported by the Starting Research Grant for High-level Talents from Guangxi University and the Postdoctoral Project from Guangxi University. Authors would like to thank Guangxi University, Prince Sattam Bin Abdulaziz University and University of Leuven for providing necessary facilities to conduct this research.

Appendix A. Supplementary data

Supplementary data to this article can be found online at https://doi.org/10.1016/j.jpha.2020.08.012.

References

[1] G. Lu, Q. Wang, G.F. Gao, Bat-to-human: spike features determining 'host jump'of coronaviruses SARS-CoV, MERS-CoV, and beyond, Trends Microbiol. 23 (2015) 468–478.
[2] T. Ahmed, M. Noman, A. Almatroudi, et al., Coronavirus disease 2019 associated pneumonia in China: current status and future prospects, Preprints (2020). https://doi.org/10.20944/preprints202002.0358.v3.
[3] L.-F. Wang, P.J. Walker, L.L. Poon, Mass extinctions, biodiversity and mitochondrial function: are bats 'special'as reservoirs for emerging viruses? Curr. Opin. Virol. 1 (2011) 649–657.
[4] J.S. Mackenzie, M. Jeggo, Reservoirs and vectors of emerging viruses, Curr. Opin. Virol. 3 (2013) 170–179.
[5] Consensus document on the epidemiology of severe acute respiratory

syndrome (SARS), World Health Organization, 2003. https://apps.who.int/iris/handle/10665/70863.
[6] P. Woo, Y. Huang, S. Lau, et al., Coronavirus genomics and bioinformatics analysis, Viruses 2 (2010) 1804–1820.
[7] V.S. Raj, A.D. Osterhaus, R.A. Fouchier, et al., MERS: emergence of a novel human coronavirus, Curr. Opin. Virol. 5 (2014) 58–62.
[8] E.I. Azhar, S.A. El-Kafrawy, S.A. Farraj, et al., Evidence for camel-to-human transmission of MERS coronavirus, N. Engl. J. Med. 370 (2014) 2499–2505.
[9] P. Vijayanand, E. Wilkins, M. Woodhead, Severe acute respiratory syndrome (SARS): a review, Clin. Med. 4 (2004) 152–160.
[10] N. Ramadan, H. Shaib, Middle East respiratory syndrome coronavirus (MERS-CoV): a review, Germs 9 (2019) 35–42.
[11] C. Liu, Q. Zhou, Y. Li, et al., Research and development on therapeutic agents and vaccines for COVID-19 and related human coronavirus diseases, ACS Cent. Sci. 6 (2020) 315–331.
[12] D.-G. Ahn, H.-J. Shin, M.-h. Kim, et al., Current status of epidemiology, diagnosis, therapeutics, and vaccines for novel coronavirus disease 2019 (COVID-19), J. Microbiol. Biotechnol. 30 (2020) 313–324.
[13] L. Rosenbaum, Facing Covid-19 in Italy—ethics, logistics, and therapeutics on the epidemic's front line, N. Engl. J. Med. 382 (2020) 1873–1875.
[14] J.M. Sanders, M.L. Monogue, T.Z. Jodlowski, et al., Pharmacologic treatments for coronavirus disease 2019 (COVID-19): a review, J. Am. Med. Assoc. 323 (2020) 1824–1836.
[15] L. Wang, Y. Wang, D. Ye, et al., A review of the 2019 Novel Coronavirus (COVID-19) based on current evidence, Int. J. Antimicrob. Agents 55 (2020), 105948.
[16] X. Xu, P. Chen, J. Wang, et al., Evolution of the novel coronavirus from the ongoing Wuhan outbreak and modeling of its spike protein for risk of human transmission, Sci. China Life Sci. 63 (2020) 457–460.
[17] N. Zhu, D. Zhang, W. Wang, et al., A novel coronavirus from patients with pneumonia in China, 2019, N. Engl. J. Med. 382 (2020) 727–733.
[18] K. Ratia, K.S. Saikatendu, B.D. Santarsiero, et al., Severe acute respiratory syndrome coronavirus papain-like protease: structure of a viral deubiquitinating enzyme, PNAS USA 103 (2006) 5717–5722.
[19] Y.M. Báez-Santos, S.E.S. John, A.D. Mesecar, The SARS-coronavirus papain-like protease: structure, function and inhibition by designed antiviral compounds, Antivir. Res. 115 (2015) 21–38.
[20] M.U. Mirza, S. Ahmad, I. Abdullah, et al., Identification of novel human USP2 inhibitor: might involve in SARS-CoV-2 papain-like (PLpro) protease deubiquitination activity, Preprints (2020). https://doi.org/10.20944/preprints202005.0136.v1.
[21] K. Ratia, S. Pegan, J. Takayama, et al., A noncovalent class of papain-like protease/deubiquitinase inhibitors blocks SARS virus replication, PNAS USA 105 (2008) 16119–16124.
[22] C. Wu, Y. Liu, Y. Yang, et al., Analysis of therapeutic targets for SARS-CoV-2 and discovery of potential drugs by computational methods, Acta Pharm. Sin. B 10 (2020) 766–788.
[23] D.S. Hui, E. I Azhar, T.A. Madani, et al., The continuing 2019-nCoV epidemic threat of novel coronaviruses to global health—the latest 2019 novel coronavirus outbreak in Wuhan, China, Int. J. Infect. Dis. 91 (2020) 264–266.
[24] M. Tahir ul Qamar, F. Shahid, U.A. Ashfaq, et al., Structural modeling and conserved epitopes prediction against SARS-COV-2 structural proteins for vaccine development, Research Square (2020). https://doi.org/10.21203/rs.2.23973/v1.
[25] C.I. Paules, H.D. Marston, A.S. Fauci, Coronavirus infections—more than just the common cold, J. Am. Med. Assoc. 323 (2020) 707–708.
[26] M. Wang, R. Cao, L. Zhang, et al., Remdesivir and chloroquine effectively inhibit the recently emerged novel coronavirus (2019-nCoV) in vitro, Cell Res. 30 (2020) 269–271.
[27] W. Liu, J.S. Morse, T. Lalonde, et al., Learning from the past: possible urgent prevention and treatment options for severe acute respiratory infections caused by 2019-nCoV, Chembiochem 21 (2020) 730–738.
[28] M. Tahir ul Qamar, A. Maryam, I. Muneer, et al., Computational screening of medicinal plant phytochemicals to discover potent pan-serotype inhibitors against dengue virus, Sci. Rep. 9 (2019) 1–16.
[29] M. Tahir Ul Qamar, S. Saleem, U.A. Ashfaq, et al., Epitope-based peptide vaccine design and target site depiction against Middle East Respiratory Syndrome Coronavirus: an immune-informatics study, J. Transl. Med. 17 (2019), 362.
[30] M.U. Mirza, M. Froeyen, Structural elucidation of SARS-CoV-2 vital proteins: computational methods reveal potential drug candidates against Main protease, Nsp12 RNA-dependent RNA polymerase and Nsp13 helicase, J. Pharm. Anal. 10 (2020) 320–328.
[31] M.U. Mirza, N. Ikram, Integrated computational approach for virtual hit identification against ebola viral proteins VP35 and VP40, Int. J. Mol. Sci. 17 (2016), 1748.
[32] I. Muneer, M. Tahir Ul Qamar, K. Tusleem, et al., Discovery of selective inhibitors for cyclic AMP response element-binding protein: a combined ligand and structure-based resources pipeline, Anti Canc. Drugs 30 (2019) 363–373.
[33] H. Khalid, K.B. Landry, B. Ijaz, et al., Discovery of novel Hepatitis C virus inhibitor targeting multiple allosteric sites of NS5B polymerase, Infect. Genet. Evol. 84 (2020), 104371.
[34] N.A. Saleh, The QSAR and docking calculations of fullerene derivatives as HIV-1 protease inhibitors, Spectrochim, Acta Part A: Molecular and Biomolecular Spectroscopy 136 (2015) 1523–1529.
[35] M.U. Mirza, M. Vanmeert, A. Ali, et al., Perspectives towards antiviral drug discovery against Ebola virus, J. Med. Virol. 91 (2019) 2029–2048.
[36] M.U. Mirza, M. Vanmeert, M. Froeyen, et al., In silico structural elucidation of RNA-dependent RNA polymerase towards the identification of potential Crimean-Congo Hemorrhagic Fever Virus inhibitors, Sci. Rep. 9 (2019) 1–18.
[37] S. Durdagi, M.T. ul Qamar, R.E. Salmas, et al., Investigating the molecular mechanism of staphylococcal DNA gyrase inhibitors: a combined ligand-based and structure-based resources pipeline, J. Mol. Graph. Model. 85 (2018) 122–129.
[38] M. Tahir ul Qamar, U.A. Ashfaq, K. Tusleem, et al., In-silico identification and evaluation of plant flavonoids as dengue NS2B/NS3 protease inhibitors using molecular docking and simulation approach, Pak. J. Pharm. Sci. 30 (2017) 2119–2137.
[39] J. Du, T.A. Cross, H.-X. Zhou, Recent progress in structure-based anti-influenza drug design, Drug Discov. Today 17 (2012) 1111–1120.
[40] P.B. Madrid, S. Chopra, I.D. Manger, et al., A systematic screen of FDA-approved drugs for inhibitors of biological threat agents, PloS One 8 (2013), e60579.
[41] M.U. Mirza, N. Ikram, Integrated computational approach for virtual hit identification against ebola viral proteins VP35 and VP40, Int. J. Mol. Sci. 17 (2016), 1748.
[42] A.C. Shurtleff, T.L. Nguyen, D.A. Kingery, et al., Therapeutics for filovirus infection: traditional approaches and progress towards in silico drug design, Expet Opin. Drug Discov. 7 (2012) 935–954.
[43] S.L. Leela, C. Srisawat, G.P. Sreekanth, et al., Drug repurposing of minocycline against dengue virus infection, Biochem. Biophys. Res. Commun. 478 (2016) 410–416.
[44] V. Luzhkov, E. Decroly, B. Canard, et al., Evaluation of adamantane derivatives as inhibitors of dengue virus mRNA cap methyltransferase by docking and molecular dynamics simulations, Mol. Inform. 32 (2013) 155–164.
[45] Q.Y. Wang, S.J. Patel, E. Vangrevelinghe, et al., A small-molecule dengue virus entry inhibitor, Antimicrob. Agents Chemother. 53 (2009) 1823–1831.
[46] Z. Zhou, M. Khaliq, J.-E. Suk, et al., Antiviral compounds discovered by virtual screening of Small– molecule libraries against dengue virus E protein, ACS Chem. Biol. 3 (2008) 765–775.
[47] P. Parida, L.M. Nainwal, A. Das, et al., Potential of plant alkaloids as dengue ns3 protease inhibitors: molecular docking and simulation approach, Bangladesh J. Pharmacol. 9 (2014) 262–267.
[48] M. Tahir ul Qamar, S. Kiran, U.A. Ashfaq, et al., Discovery of novel dengue NS2B/NS3 protease inhibitors using pharmacophore modeling and molecular docking based virtual screening of the zinc database, Int. J. Pharmacol. 12 (2016) 621–632.
[49] C. Nitsche, Strategies towards Protease Inhibitors for Emerging Flaviviruses, Dengue and Zika: Control and Antiviral Treatment Strategies, Springer, 2018, pp. 175–186.
[50] A. Pattnaik, N. Palermo, B.R. Sahoo, et al., Discovery of a non-nucleoside RNA polymerase inhibitor for blocking Zika virus replication through in silico screening, Antivir. Res. 151 (2018) 78–86.
[51] R. Ramajayam, K.-P. Tan, H.-G. Liu, et al., Synthesis, docking studies, and evaluation of pyrimidines as inhibitors of SARS-CoV 3CL protease, Bioorg. Med. Chem. Lett 20 (2010) 3569–3572.
[52] L. Wang, B.-B. Bao, G.-Q. Song, et al., Discovery of unsymmetrical aromatic disulfides as novel inhibitors of SARS-CoV main protease: chemical synthesis, biological evaluation, molecular docking and 3D-QSAR study, Eur. J. Med. Chem. 137 (2017) 450–461.
[53] M. Tahir ul Qamar, S.M. Alqahtani, M.A. Alamri, et al., Structural basis of SARS-CoV-2 3CLpro and anti-COVID-19 drug discovery from medicinal plants, J. Pharm. Anal. 10 (2020) 313–319.
[54] T. Hou, R. Yu, Molecular dynamics and free energy studies on the wild-type and double mutant HIV-1 protease complexed with amprenavir and two amprenavir-related inhibitors: mechanism for binding and drug resistance, J. Med. Chem. 50 (2007) 1177–1188.
[55] J. Tu, J.J. Li, Z.J. Shan, et al., Exploring the binding mechanism of Heteroaryldihydropyrimidines and Hepatitis B Virus capsid combined 3D-QSAR and molecular dynamics, Antivir. Res. 137 (2017) 151–164.
[56] S. Anusuya, M.M. Gromiha, Quercetin derivatives as non-nucleoside inhibitors for dengue polymerase: molecular docking, molecular dynamics simulation, and binding free energy calculation, J. Biomol. Struct. Dyn. 35 (2017) 2895–2909.
[57] S. Guan, T. Wang, Z. Kuai, et al., Exploration of binding and inhibition mechanism of a small molecule inhibitor of influenza virus H1N1 hemagglutinin by molecular dynamics simulation, Sci. Rep. 7 (2017), 3786.
[58] S. Bhakat, A.J. Martin, M.E. Soliman, An integrated molecular dynamics, principal component analysis and residue interaction network approach reveals the impact of M184V mutation on HIV reverse transcriptase resistance to lamivudine, Mol. Biosyst. 10 (2014) 2215–2228.
[59] B. Speelman, B.R. Brooks, C.B. Post, Molecular dynamics simulations of human rhinovirus and an antiviral compound, Biophys. J. 80 (2001) 121–129.
[60] M. Mottin, R.C. Braga, R.A. da Silva, et al., Molecular dynamics simulations of Zika virus NS3 helicase: insights into RNA binding site activity, Biochem. Biophys. Res. Commun. 492 (2017) 643–651.
[61] C. Zhang, T. Feng, J. Cheng, et al., Structure of the NS5 methyltransferase from Zika virus and implications in inhibitor design, Biochem. Biophys. Res. Commun. 492 (2017) 624–630.
[62] D. Pan, Y. Niu, W. Xue, et al., Computational study on the drug resistance

mechanism of hepatitis C virus NS5B RNA-dependent RNA polymerase mutants to BMS-791325 by molecular dynamics simulation and binding free energy calculations, Chemometr. Intell. Lab. Syst. 154 (2016) 185–193.
[63] G. Leonis, T. Steinbrecher, M.G. Papadopoulos, A contribution to the drug resistance mechanism of Darunavir, Amprenavir, Indinavir, and Saquinavir complexes with HIV-1 protease due to flap mutation I50V: a systematic MM–PBSA and thermodynamic integration study, J. Chem. Inf. Model. 53 (2013) 2141–2153.
[64] P. Pan, L. Li, Y. Li, et al., Insights into susceptibility of antiviral drugs against the E119G mutant of 2009 influenza A (H1N1) neuraminidase by molecular dynamics simulations and free energy calculations, Antivir. Res. 100 (2013) 356–364.
[65] C. McInnes, Virtual screening strategies in drug discovery, Curr. Opin. Chem. Biol. 11 (2007) 494–502.
[66] H.M. Berman, P.E. Bourne, J. Westbrook, et al., The Protein Data Bank, Protein Structure, CRC Press, 2003, pp. 394–410.
[67] F. Sievers, A. Wilm, D. Dineen, et al., Fast, scalable generation of high-quality protein multiple sequence alignments using Clustal Omega, Mol. Syst. Biol. 7 (2011), 539.
[68] W.L. DeLano, Pymol: an open-source molecular graphics tool, CCP4 Newslett. Protein Crystallogr. 40 (2002) 82–92.
[69] N.M. O'Boyle, M. Banck, C.A. James, et al., Open Babel: an open chemical toolbox, J. Cheminf. 3 (2011), 33.
[70] S. Forli, R. Huey, M.E. Pique, et al., Computational protein–ligand docking and virtual drug screening with the AutoDock suite, Nat. Protoc. 11 (2016) 905–919.
[71] D. Systèmes, BIOVIA, Discovery Studio Modeling Environment, Dassault Systèmes Biovia, San Diego, CA, USA, 2016.
[72] S. Dallakyan, A.J. Olson, Small-Molecule Library Screening by Docking with PyRx, in: J. Hempel, C. Williams, C. Hong (eds.), Chemical Biology, Methods in Molecular Biology, Vol. 1263, Humana Press, New York, 2015. https://doi.org/10.1007/978-1-4939-2269-7_19.
[73] Q. Wang, J. He, D. Wu, et al., Interaction of α-cyperone with human serum albumin: determination of the binding site by using Discovery Studio and via spectroscopic methods, J. Lumin. 164 (2015) 81–85.
[74] A. Daina, O. Michielin, V. Zoete, SwissADME: a free web tool to evaluate pharmacokinetics, drug-likeness and medicinal chemistry friendliness of small molecules, Sci. Rep. 7 (2017), 42717.
[75] B. Gimenez, M. Santos, M. Ferrarini, et al., Evaluation of blockbuster drugs under the rule-of-five, Pharmazie-Int. J. Pharm. Sci. 65 (2010) 148–152.
[76] D.E.V. Pires, T.L. Blundell, D.B. Ascher, pkCSM: predicting small-molecule pharmacokinetic and toxicity properties using graph-based signatures, J. Med. Chem. 58 (2015) 4066–4072.
[77] B. Hess, C. Kutzner, D. Van Der Spoel, et al., Gromacs 4: algorithms for highly efficient, load-balanced, and scalable molecular simulation, J. Chem. Theor. Comput. 4 (2008) 435–447.
[78] M.A. Alamri, Pharmacoinformatics and molecular dynamic simulation studies to identify potential small-molecule inhibitors of WNK-SPAK/OSR1 signaling that mimic the RFQV motifs of WNK kinases, Arabian J. Chem. 13 (2020) 5107–5117.
[79] E.C. Meng, E.F. Pettersen, G.S. Couch, et al., Tools for integrated sequence-structure analysis with UCSF Chimera, BMC Bioinf. 7 (2006), 339.
[80] B.R. Miller Iii, T.D. McGee Jr., J.M. Swails, et al., MMPBSA. py: an efficient program for end-state free energy calculations, J. Chem. Theor. Comput. 8 (2012) 3314–3321.
[81] N. Ikram, M.U. Mirza, M. Vanmeert, et al., Inhibition of oncogenic kinases: an in vitro validated computational approach identified potential multi-target anticancer compounds, Biomolecules 9 (2019), 124.
[82] K. Iman, M.U. Mirza, N. Mazhar, et al., In silico structure-based identification of novel acetylcholinesterase inhibitors against alzheimer's disease, CNS Neurol. Disord. Drug Targets 17 (2018) 54–68.
[83] T. Hou, J. Wang, Y. Li, et al., Assessing the performance of the MM/PBSA and MM/GBSA methods. 1. The accuracy of binding free energy calculations based on molecular dynamics simulations, J. Chem. Inf. Model. 51 (2011) 69–82.
[84] H.K. Srivastava, G.N. Sastry, Molecular dynamics investigation on a series of HIV protease inhibitors: assessing the performance of MM-PBSA and MM-GBSA approaches, J. Chem. Inf. Model. 52 (2012) 3088–3098.
[85] J.J. Tan, W. Zu Chen, C.X. Wang, Investigating interactions between HIV-1 gp41 and inhibitors by molecular dynamics simulation and MM–PBSA/GBSA calculations, J. Mol. Struct.: THEOCHEM 766 (2006) 77–82.
[86] J.F. Chan, K.-H. Chan, R.Y. Kao, et al., Broad-spectrum antivirals for the emerging Middle East respiratory syndrome coronavirus, J. Infect. 67 (2013) 606–616.
[87] A.K. Ghosh, J. Takayama, K.V. Rao, et al., Severe acute respiratory syndrome coronavirus papain-like novel protease inhibitors: design, synthesis, protein– ligand X-ray structure and biological evaluation, J. Med. Chem. 53 (2010) 4968–4979.
[88] M. Tahir ul Qamar, Z. Shokat, I. Muneer, et al., Multiepitope-based subunit vaccine design and evaluation against respiratory syncytial virus using reverse vaccinology approach, Vaccines 8 (2020), 288.
[89] M.A. Alamri, M. Tahir ul Qamar, M.U. Mirza, et al., Pharmacoinformatics and molecular dynamics simulation studies reveal potential covalent and FDA-approved inhibitors of SARS-CoV-2 main protease $3CL^{pro}$, J. Biomol. Struct. Dyn. (2020) 1–13.
[90] K. El Hage, P. Mondal, M. Meuwly, Free energy simulations for protein ligand binding and stability, Mol. Simulat. 44 (2018) 1044–1061.
[91] K. Liu, H. Kokubo, Exploring the stability of ligand binding modes to proteins by molecular dynamics simulations: a cross-docking study, J. Chem. Inf. Model. 57 (2017) 2514–2522.
[92] K. Liu, E. Watanabe, H. Kokubo, Exploring the stability of ligand binding modes to proteins by molecular dynamics simulations, J. Comput. Aided Mol. Des. 31 (2017) 201–211.
[93] M. Wieder, U. Perricone, S. Boresch, et al., Evaluating the stability of pharmacophore features using molecular dynamics simulations, Biochem. Biophys. Res. Commun. 470 (2016) 685–689.
[94] L. McGillewie, M.E. Soliman, The binding landscape of plasmepsin V and the implications for flap dynamics, Mol. Biosyst. 12 (2016) 1457–1467.
[95] T. Sindhu, P. Srinivasan, Exploring the binding properties of agonists interacting with human TGR5 using structural modeling, molecular docking and dynamics simulations, RSC Adv. 5 (2015) 14202–14213.
[96] T.J. Richmond, Solvent accessible surface area and excluded volume in proteins: analytical equations for overlapping spheres and implications for the hydrophobic effect, J. Mol. Biol. 178 (1984) 63–89.
[97] F. Chen, H. Liu, H. Sun, et al., Assessing the performance of the MM/PBSA and MM/GBSA methods. 6. Capability to predict protein–protein binding free energies and re-rank binding poses generated by protein–protein docking, Phys. Chem. Chem. Phys. 18 (2016) 22129–22139.
[98] S. Sirin, R. Kumar, C. Martinez, et al., A computational approach to enzyme design: predicting ω-aminotransferase catalytic activity using docking and MM-GBSA scoring, J. Chem. Inf. Model. 54 (2014) 2334–2346.
[99] T. Hou, J. Wang, Y. Li, et al., Assessing the performance of the MM/PBSA and MM/GBSA methods. 1. The accuracy of binding free energy calculations based on molecular dynamics simulations, J. Chem. Inf. Model. 51 (2011) 69–82.
[100] H. Sun, L. Duan, F. Chen, et al., Assessing the performance of MM/PBSA and MM/GBSA methods. 7. Entropy effects on the performance of end-point binding free energy calculation approaches, Phys. Chem. Chem. Phys. 20 (2018) 14450–14460.
[101] M.-H. Lin, D.C. Moses, C.-H. Hsieh, et al., Disulfiram can inhibit mers and sars coronavirus papain-like proteases via different modes, Antivir. Res. 150 (2018) 155–163.
[102] G. Li, E. De Clercq, Therapeutic options for the 2019 novel coronavirus (2019-nCoV), Nat. Rev. Drug Discov. 19 (2020) 149–150.
[103] T. Bobrowski, V. Alves, C.C. Melo-Filho, et al., Computational models identify several FDA approved or experimental drugs as putative agents against SARS-CoV-2, ChemRxiv. (2020), https://doi.org/10.26434/chemrxiv.12153594.v1.
[104] F. Hu, J. Jiang, P. Yin, Prediction of Potential Commercially Inhibitors against SARS-CoV-2 by Multi-Task Deep Model, arXiv preprint, 2020. https://arxiv.org/abs/2003.00728.
[105] J.F. Chan, K.-H. Chan, R.Y. Kao, et al., Broad-spectrum antivirals for the emerging Middle East respiratory syndrome coronavirus, J. Infect. 67 (2013) 606–616.
[106] J.F.-W. Chan, Y. Yao, M.-L. Yeung, et al., Treatment with lopinavir/ritonavir or interferon-β1b improves outcome of MERS-CoV infection in a nonhuman primate model of common marmoset, J. Infect. Dis. 212 (2015) 1904–1913.
[107] Y.M. Arabi, A. Alothman, H.H. Balkhy, et al., Treatment of Middle East Respiratory Syndrome with a combination of lopinavir-ritonavir and interferon-β1b (MIRACLE trial): study protocol for a randomized controlled trial, Trials 19 (2018), 81.
[108] T.P. Sheahan, A.C. Sims, S.R. Leist, et al., Comparative therapeutic efficacy of remdesivir and combination lopinavir, ritonavir, and interferon beta against MERS-CoV, Nat. Commun. 11 (2020) 1–14.
[109] C. Chu, V. Cheng, I. Hung, et al., Role of lopinavir/ritonavir in the treatment of SARS: initial virological and clinical findings, Thorax 59 (2004) 252–256.
[110] V. Nukoolkarn, V.S. Lee, M. Malaisree, et al., Molecular dynamic simulations analysis of ritronavir and lopinavir as SARS-CoV 3CLpro inhibitors, J. Theor. Biol. 254 (2008) 861–867.
[111] L.J. Stockman, R. Bellamy, P. Garner, SARS: systematic review of treatment effects, PLoS Med. 3 (2006), e343.
[112] T.T. Yao, J.D. Qian, W.Y. Zhu, et al., A systematic review of lopinavir therapy for SARS coronavirus and MERS coronavirus—A possible reference for coronavirus disease-19 treatment option, J. Med. Virol. 92 (2020) 556–563.
[113] I.F.-N. Hung, K.-C. Lung, E.Y.-K. Tso, et al., Triple combination of interferon beta-1b, lopinavir–ritonavir, and ribavirin in the treatment of patients admitted to hospital with COVID-19: an open-label, randomised, phase 2 trial, Lancet 395 (2020) 1695–1704.
[114] S. Moro, G. Bolcato, M. Bissaro, et al., Targeting the Coronavirus SARS-CoV-2: computational insights into the mechanism of action of the protease inhibitors Lopinavir, Ritonavir, and Nelfinavir, Research Square (2020). https://doi.org/10.21203/rs.3.rs-20948/v1.
[115] M. Hurst, D. Faulds, Lopinavir, Drugs 60 (2000) 1371–1379.
[116] H. Lee, H. Lei, B.D. Santarsiero, et al., Inhibitor recognition specificity of MERS-CoV papain-like protease may differ from that of SARS-CoV, ACS Chem. Biol. 10 (2015) 1456–1465.
[117] L. Cregar-Hernandez, G.-S. Jiao, A.T. Johnson, et al., Small molecule pan-dengue and West Nile virus NS3 protease inhibitors, Antiviral Chem. Chemother. 21 (2011) 209–217.
[118] B. Lin, S. He, H.J. Yim, et al., Evaluation of antiviral drug synergy in an

infectious HCV system, Antivir. Ther. 21 (2016) 595–603.
[119] D.A. DeGoey, J.T. Randolph, D. Liu, et al., Discovery of ABT-267, a pan-genotypic inhibitor of HCV NS5A, J. Med. Chem. 57 (2014) 2047–2057.
[120] A.M. Lam, E. Murakami, C. Espiritu, et al., PSI-7851, a pronucleotide of β-D-2′-deoxy-2′-fluoro-2′-C-methyluridine monophosphate, is a potent and pan-genotype inhibitor of hepatitis C virus replication, Antimicrob. Agents Chemother. 54 (2010) 3187–3196.
[121] M. Belema, N.A. Meanwell, Discovery of daclatasvir, a pan-genotypic hepatitis C virus NS5A replication complex inhibitor with potent clinical effect, J. Med. Chem. 57 (2014) 5057–5071.
[122] H. Nakata, S.M. Steinberg, Y. Koh, et al., Potent synergistic anti-human immunodeficiency virus (HIV) effects using combinations of the CCR5 inhibitor aplaviroc with other anti-HIV drugs, Antimicrob. Agents Chemother. 52 (2008) 2111–2119.